POLITECNICO DI TORINO
Repository ISTITUZIONALE

The ICRF antenna of DTT: Design status and perspectives

(Article begins on next page)

28 April 2024

The ICRF Antenna of DTT: Design Status and Perspectives

S. Ceccuzzi,[1, 2, a)] B. Baiocchi,[3, b)] A. Cardinali,[2, c)] G. Di Gironimo,[1, 4, 5, d)]
G. Granucci,[3, e)] D. Liuzza,[2, f)] D. Mascali,[6, g)] G. S. Mauro,[6, h)] D. Milanesio,[7, i)]
F. Mirizzi,[4, j)] A. Pidatella,[6, k)] S. Piras,[2, l)] C. Ponti,[8, m)] G. L. Ravera,[2, n)]
G. Schettini,[8, o)] G. Torrisi,[6, p)] A. A. Tuccillo,[1, 4, q)] and G. Vecchi[7, r)]

[1)]*DTT S.C. a r.l., Via Enrico Fermi 45, 00044, Frascati, Italy.*
[2)]*ENEA, Via Enrico Fermi 45, 00044, Frascati, Italy.*
[3)]*CNR-ISTP, Via Roberto Cozzi 53, 20125, Milano, Italy.*
[4)]*CREATE, Via Claudio 21, 80125, Napoli, Italy.*
[5)]*Università degli Studi di Napoli Federico II, Corso Umberto I 40, 80138, Napoli, Italy.*
[6)]*INFN-LNS, Via Santa Sofia 62, 95123, Catania, Italy.*
[7)]*Politecnico di Torino, Corso Duca degli Abruzzi 24, 10129, Torino, Italy.*
[8)]*Università degli Studi Roma Tre, Via Vito Volterra 62, 00146, Roma, Italy.*

[a)]*Corresponding author: silvio.ceccuzzi@enea.it*
[b)]*Electronic mail: benedetta.baiocchi@istp.cnr.it*
[c)]*Electronic mail: alessandro.cardinali@enea.it*
[d)]*Electronic mail: giuseppe.digironimo@unina.it*
[e)]*Electronic mail: gustavo.granucci@istp.cnr.it*
[f)]*Electronic mail: davide.liuzza@enea.it*
[g)]*Electronic mail: davidmascali@lns.infn.it*
[h)]*Electronic mail: mauro@lns.infn.it*
[i)]*Electronic mail: daniele.milanesio@polito.it*
[j)]*Electronic mail: francesco.mirizzi@outlook.it*
[k)]*Electronic mail: pidatella@lns.infn.it*
[l)]*Electronic mail: sebastian.piras@enea.it*
[m)]*Electronic mail: cristina.ponti@uniroma3.it*
[n)]*Electronic mail: gianluca.ravera@enea.it*
[o)]*Electronic mail: giuseppe.schettini@uniroma3.it*
[p)]*Electronic mail: peppetorrisi@lns.infn.it*
[q)]*Electronic mail: angelo.tuccillo@dtt-project.it*
[r)]*Electronic mail: giuseppe.vecchi@polito.it*

Abstract. The basis of design for the Ion Cyclotron Range of Frequency (ICRF) antennas of the Divertor Tokamak Test facility (DTT) is defined and the most suitable design solutions abiding by such requirements are shown. DTT antenna has to reliably couple a radiofrequency (RF) power $\geq$1.5 MW in the range 60$\div$90 MHz to the single-null, 6 T, 5.5 MA, DTT scenario and allow for remote (dis)assembling and maintenance operations of its plasma-facing components. Most documented antenna concepts are considered and a large set of alternatives, based on toroidal arrays of two, three or four straps with different shapes and constraints, is quantitatively assessed in terms of RF performances. Two most promising candidates are identified: the one, selected to access a detailed design phase, relies on traditional radiating elements, the other is an innovative concept requiring some R&D.

INTRODUCTION

The Ion Cyclotron Radio Frequency (ICRF) has been an additional plasma heating method in magnetic confinement fusion machines for more than 50 years [1]. ICRF systems are an essential tool in most of existing tokamaks and new deployments are planned or under investigation, e.g. for CFETR [2], DEMO [3], ITER [4], SPARC [5], and W7-X [6]. An ICRF system is to be designed also for the Divertor Tokamak Test facility (DTT) [7], a new tokamak under realization at the ENEA Frascati Research Center with main parameters: B_0 =6 T, I_p =5.5 MA, R_0 =2.19 m, a =0.7 m, and pulse length around 100 s. DTT aims at studying integrated heat-exhaust systems capable of withstanding the large power loads in the European DEMO through a considerable flexibility in terms of magnetic configurations. The DTT additional heating power mostly relies on electron cyclotron (EC) waves and, to a smaller extent, on ICRF and neutral beam injection (NBI). The heating systems will be progressively deployed up to a power level of 45 MW with the final mix not frozen yet. Depending on the achievements or troubles with the first installations, the total ICRF system may consist of two, four or six antennas.
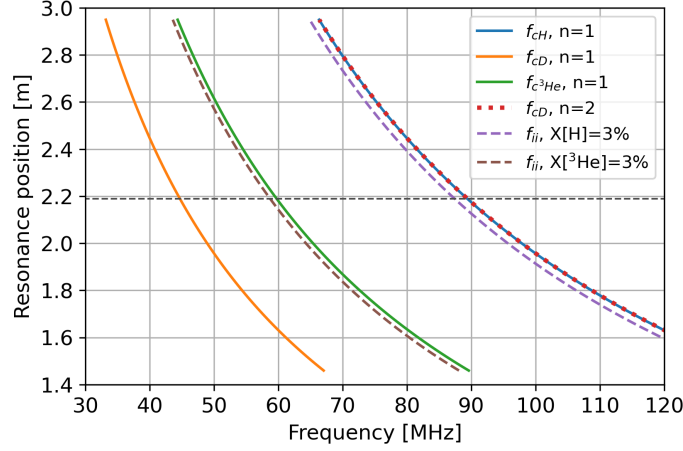
FIGURE 1. Radial position of cyclotron and ion-ion resonance frequencies in DTT for a vacuum toroidal field of 5.85 T at the geometrical axis. Deuterium majority is assumed for two-ion resonances.

The design of radiofrequency (RF) antennas is an intensive research topic owing to the constant endeavour to increase coupling performance, to reduce plasma wall interaction, and to improve resilience against fast changes in the loading, while withstanding in-vessel harsh environment. Developed solutions include use of vacuum capacitors [8], short straps fed with poloidal splitters [4], magnetic field alignment (FA) [9], cancellation of RF image currents [10], and travelling wave concepts [11] just to cite a few. Furthermore, as in reactor-relevant machines, the plasma-facing components (PFC) of DTT will undergo activation after operations at full power, preventing manual intervention on PFC for a long time.

A preliminary investigation of the ICRF antennas for DTT [12] opted for a sturdy, port-plug solution based on 2 (toroidal) x 4 (poloidal) short straps fed by 3-port junctions. Since then, DTT underwent some modifications, making such solution incompatible with the final port size, and research advancements suggested to sacrifice design simplicity in favour of a reduction in ICRF-related PFC sputtering [13]. A design group has been thus formed to select the most suitable antenna concept for DTT on a quantitative basis, without necessarily preferring simple mechanical solutions. This paper reports the work carried out within this group, starting from the initial requirements, providing a brief description of the entire system, and explaining adopted approach and outcomes.

BASIS OF DESIGN

Physics requirements and system overview

The ICRF system of DTT is primarily intended for heating of bulk ions, H-mode access, and wall cleaning. Another important application, where ICRF is expected to play an important role, is the generation of fast particles. A helpful but optional contribution is instead foreseen with reference to other tasks feasible with symmetrical spectra like assisted startup, electron heating, control of impurity accumulation, current profile control, etc., whereas applications based on directional waves, e.g. current drive, are out of system scope.

The heating of ^{3}He or H minorities is considered the preferred ICRF scheme to allow DTT to accomplish its main mission. A frequency range from 60 to 90 MHz has been chosen to this aim on the basis of Fig. 1, where the position of the resonance layers are depicted as a function of the antenna frequency for the adopted $B_0 = 5.85$ T. Ion cyclotron wall cleaning and wall conditioning (ICWC) can rely on several recipes [14], some of which are feasible within the selected frequency range. ICRF can profitably contribute to the generation of fast ions at 60 and 90 MHz via minority heating. The use of a three-ion heating scheme [15] is being explored, anyhow the chosen frequency range is compatible with it in the case of D-H-^{3}He plasmas. As far as the parallel refractive index $n_\parallel$ is concerned, no stringent requirements are prescribed. Linear absorption by minority ions slightly increases for low $n_\parallel$ [16] and ICWC can efficiently work even with monopole antenna phasing.
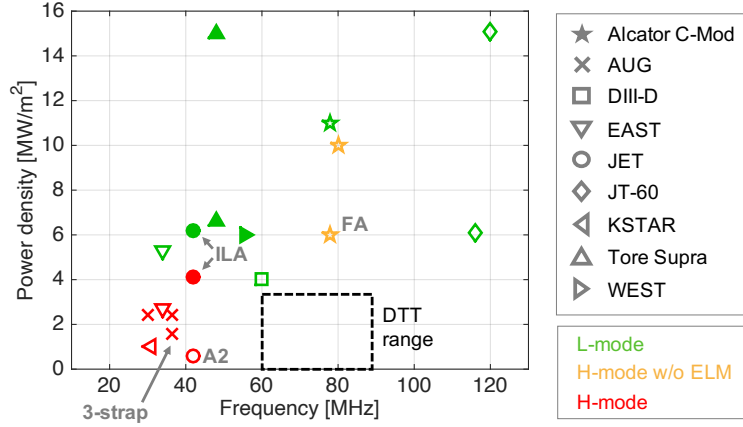
FIGURE 2. Power densities of ICRF antennas vs. frequency reported or derived from literature and private communications. Filled markers denote antennas with in-vessel capacitors. The authors apologize for any inaccuracy.
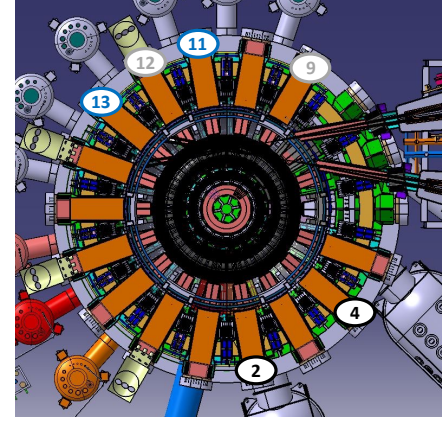

FIGURE 3. DTT sectors with ICRF ports in the case of two (black), four (black + blue) and six (black + blue + grey) antennas.

According to integrated modeling simulations [17], the optimal RF power to be coupled to the DTT single-null scenario is 6 MW. A larger ICRF power, i.e. 9 MW, added at the expenses of EC heating, produces negligible impact on ion temperature, while the effect of far higher power (>10 MW) was not assessed owing to its demanding implications, clarified hereinafter, on the number of ICRF ports. The injection of ICRF power is planned during the plasma current plateau, which means RF pulses of maximum 50 s every hour. Experiments with fast ions in D(H) plasmas are already feasible with an ICRF power of 6 MW [18], whereas D(^{3}He) plasmas require at least 9 MW or other scenarios yet to be explored, e.g. based on the 3-ion heating scheme or on a synergy with the NBI. With reference to ICWC, its operational requirements have been derived with some safety margin from scientific literature, resulting in 200 kW continuous wave delivered to the DTT torus [19].

Allowable sizes for the radiating area of ICRF antennas in DTT are approximately in the range from 0.3 m^2 (port-plug option) to 0.5 m^2 (remote-handling option), assuming the use of equatorial ports, which are the biggest. Realistic values for the power densities of ICRF antennas can be inferred from Fig. 2 that depicts achieved power densities by many different antennas. Net of possible small inaccuracies, it stands out that routine operations during ELMy H-mode plasmas have to be envisaged below 4 MW/m^2, being 4.1 MW/m^2 the record attained by a JET antenna with in-vessel capacitors [20], widely known with the name of ITER-like antenna (ILA). A coupled power of 1.5 MW per antenna was thus fixed for DTT, appearing an acceptable compromise between the number of ICRF ports and antenna power density. Fig. 3 shows DTT sectors with ICRF antennas for the three possible heating configurations.

The ICRF system of DTT is organized in modules, each one consists of two antennas and is expected to couple at least 3 MW to the DTT single-null reference scenario in the frequency range 60–90 MHz. Among consolidated, ELM-resilent matching schemes [21], the use of 3 dB hybrid couplers, with output branches feeding different antennas, was preferred to the external conjugate-T because it was estimated cheaper, while internal conjugate-T was discarded for the reason explained in next section. Assuming an antenna and transmission line efficiency of 70%, either two or four RF generators are required to provide an output power larger than 4.3 MW with VSWR≤1.5. There is no cavity amplifier tailored to such needs; moreover, no grid tube can deliver more than 2 MW, and no high-power tetrode presents a constant output power between 60 and 90 MHz. The eventual choice was for the development of solid-state transmitters with an output power of 1.2 MW, considering the extraordinary recent advancements and future prospects of this technology [22]. A simplified RF circuit of the ICRF system is sketched in Fig. 4. In the case of antennas with three or more straps, one pair of RF generators feeds the central straps of both antennas, while the other pair feeds their lateral straps. Close to the antenna the characteristic impedance of the transmission line passes from 50 Ω to 30 Ω; the exact location of the transition is to be decided yet.
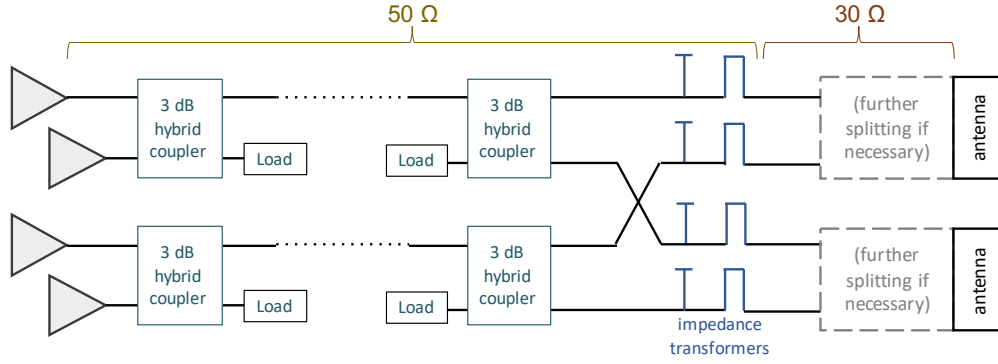
50 Ω   30 Ω

3 dB hybrid coupler   3 dB hybrid coupler   (further splitting if necessary)   antenna

Load   Load

3 dB hybrid coupler   3 dB hybrid coupler   (further splitting if necessary)   antenna

Load   Load

impedance transformers

FIGURE 4. Simplified scheme of the ICRF system of DTT.

Antenna concepts

DTT presents an unprecedented combination of challenges for traditional, i.e., unmatched, ICRF antennas in comparison with existing machines. Radially movable coupling structures are required to make the antenna loading acceptable and active cooling is mandatory to withstand the heat loads for the entire, full-performance, plasma pulse. The DTT equatorial duct, whose width is 680 mm, cannot accommodate more than two straps, which is an unfavourable configuration as regards RF-related PFC sputtering. Furthermore, the power target of 1.5 MW per antenna entails power densities beyond the state of the art for any radially movable port-plug concept. To the best of authors' knowledge, the only existing antenna that is radially movable, actively cooled, and toroidally wider than its port is the 4-strap (i.e. I-port) antenna of EAST [23]. DTT adds another challenge to the latter design: the antenna has to be remotely assembled and disassembled.

Owing to their high power density and limitation to two straps, port-plug concepts based on a traditional design were deemed unworthy to be analysed. Other options were excluded a priori. Among them, there is the travelling-wave antenna [11] that, being based on a resonant coupling between adjacent straps, is a narrow-band concept, unable to cover a frequency range as large as in DTT. Solutions based on in-vessel capacitors [6, 8], provided that they can work up to 90 MHz, were also ruled out since, in the past, capacitor faults significantly impaired the availability of some systems. Folded waveguide antennas [24] were considered, but preliminary simulations showed that even 90 MHz is a too low frequency for such a technology in a DTT port. Finally toroidal arrays with more than four straps were excluded because of the lack of space to accommodate them. Preference was given to antenna solutions that feature simple and rugged shapes, operate at an optimal radial distance from the plasma, allow for the minimization of parallel RF electric field in the far scrape-off layer (SOL), and present no significant obstacles with reference to assembling and disassembling operations at least at a conceptual level. With reference to the latter point, considered candidates can be gathered in three groups:

- *Port-plug options*: an innovative self-resonant concept is only considered in this group. The antenna is a self-contained, fully metallic, cantilevered structure that can be inserted in and extracted from DTT rather easily. Due to its novelty, a R&D activity, including the test of a mockup, is necessary.

- *Options deployable through the port*: this group includes 3- and 4-strap antennas, split into parts similarly to what proposed for DEMO [3]. Each part is autonomous and fully pre-assembled is terms of cooling and RF feeding before its installation in the tokamak. This solution has never been tested and its engineering phase may reveal unexpected complications.

- *Options relying on the remote-handling system* (RHS): they consist in 3- and 4-strap antennas whose front part is handled with the RHS, similarly to JET ILA. This solution has a critical impact on interfaces, requiring RHS cutting & welding tools for cooling pipes as well as the development of suitable connectors for RF feeds.

Various implementations have been quantitatively studied for each antenna concept, optimizing their design according to the characteristic geometrical constraints of the relevant group. The optimization settings are reported in next section, while details about all implementations and their performance is described subsequently.

TABLE I. E-field limits [MV/m].			
Machine, antenna	$\perp B$	$\parallel B$	Note
C-mod, early studies [25]	5.0	0.9	
C-mod, antenna J [25]	3.5	1.0	experimental
JET, A1 [26]	---	2.2	values
JET, ILA [27]	2.5	2.5	
ITER [4]	3.0	2.0	
Tore Supra, RDL [28]	2.3	2.3	design
WEST [8]	2.0	2.0	values
W7-X [6]	---	1.5	

TABLE II. Stand-off voltages [kV].		
Machine, antenna	design	operational
AUG, 2- & 3-strap antennas [29]	30	25–30
JET, A2 [21, 26]	42	30
JT-60U [30]	---	35
C-Mod, antenna J [25]	40	35
C-Mod, antenna D&E [25]	---	35–40
Tore Supra, ILP [31]	---	40
JET, ILA [27]	45	42
C-Mod, FA [9]	---	45
ITER [4]	45	---

RF constraints and performance evaluation

The fulfillment of physics requirements is subjected to the compliance with RF constraints, i.e. electric field limits in the antenna box and the standoff voltage in the coaxial feeds. Tables I and II report the maximum E-fields and voltages experienced by some antennas or considered for their design. In the absence of experimental data relevant to DTT for both wave frequency and magnetic field, such tables were used as guideline. Taking some margin from the uppermost values adopted in ITER, the following limits were fixed: E-field magnitude lower than 2.5 MV/m and $|E_\parallel| \leq 1.5$ MV/m everywhere inside the antenna box, and standoff voltage of 35 kV.

Abiding by such limits and geometrical constraints dictated by the assembling procedure, a preliminary RF design of many antennas was optimized with different tools. With reference to the self-resonant antenna, the optimization simply regarded the S_{11} in between 60 and 90 MHz. As far as traditional antennas are concerned, the optimization was carried out with reference to an effective minimum conductance calculated for a given phasing and power balance between the straps. In detail, the phasings $0\pi 0$ and $0\pi\pi 0$ were set in the case of three and four straps, respectively. As to the power balance, the condition $P_C = P_L$ was enforced, where P_C and P_L represent the power coupled by central and lateral straps, respectively. This procedure results in a non-linear system between the amplitudes of input power waves a_i at the antenna feeds. More precisely, the output power waves b_i are firstly expressed as a function of a_i through the scattering matrix S, computed by simulation tools, and the feeding coefficients F_i, set according to wanted phasing (the index as subscript denotes the i-th of N feeds). Then the system

$$P_C = P_L \quad \rightarrow \quad \sum_{i,\,\text{central}} \frac{1}{2}\left(|a_i|^2 - |b_i|^2\right) = \sum_{i,\,\text{lateral}} \frac{1}{2}\left(|a_i|^2 - |b_i|^2\right) \quad \text{with} \quad b_i = \sum_{j=1}^{N} S_{ij}F_j|a_j|$$

is solved to derive all a_i, which allow us to calculate b_i, reflection coefficients, voltage standing wave ratios (VSWR), maximum voltages $V_{\max}$, and minimum conductances $G_{\min}$ of each feed. The latter are reduced by a scaling factor proportional to the $V_{\max}^2$ of the relevant feed, which accounts for the fact that only the feeding line with the highest VSWR works at the standoff voltage. The effective minimum conductance G_{eff}, used as figure of merit for the coupling in the present work, is the sum of all scaled $G_{\min}$ and assures the full exploitation of the installed power (see Fig. 4).

The adopted definition of coupling performance implies that some RF feeding lines operate below the standoff voltage. To check that E-fields are below safety limits, a different, more conservative condition is used, which consists in setting the maximum voltage of all RF feeding lines to $V_{\text{standoff}} = 35$ kV. In this case, the amplitudes of input waves a_i are derived solving the following system of equations:

$$\sqrt{Z_{0i}}\left(|a_i| + |b_i|\right) = V_{\text{standoff}} \quad \text{for } i = 1, 2, \ldots, N$$

where Z_{0i} is the characteristic impedance of the i-th feed. As to the self-resonant antenna, a input power of 800 kW per feed was instead set to evaluate the maximum electric fields.

The optimization approach neglects the minimization of average parallel RF electric field $\langle E_\parallel \rangle$ on the antenna lateral sides, which is considered an indicator of the RF sheath rectification mechanism responsible for enhanced ion sputtering and additional heat loads. The minimization of $\langle E_\parallel \rangle$ is left as a subsequent optimization step to be carried out for the selected antenna option. Except for the self-resonant antenna, all concepts allow for the cancellation of image currents on antenna sides [32].
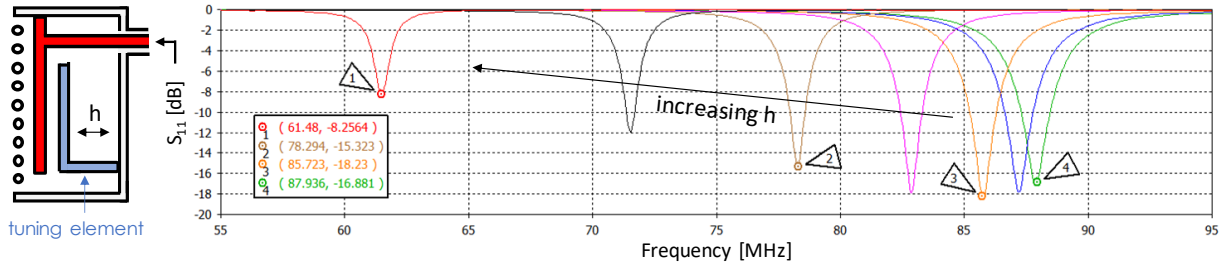
FIGURE 5. Performance of the antenna geometry sketched aside, based on the self-resonant concept.

All simulation were performed under a flat antenna approximation, i.e., neglecting poloidal and toroidal curvature. Several electromagnetic tools, modeling the antenna load with a different level of approximation, were used. Adopted types of load are an equivalent homogeneous dielectric (CST, HFSS), a 1-D non-homogeneous dielectric whose permittivity matches the squared wavenumber of the fast wave (COMSOL Multiphysics) [33], a cold slab plasma model (integrated COMSOL–Matlab environment) [34], and a hot slab plasma model (TOPICA) [35]. Antenna options were optimized with CST (or HFSS) and the performance of an optimized geometry was benchmarked with HFSS (or CST). Simulations with more realistic loads were run for the best antenna options or in the case of doubtful optimization results. In general a very good agreement was obtained between simulation tools, net of the limits of their different approximations. This activity offered the chance to improve some tools available in the design team; such modeling advancements are described in a dedicated paper [36].

Concerning the equivalent, homogeneous, dielectric load adopted for the optimization of antenna geometries, its parameters were tailored to reproduce the TOPICA results of a 3-strap antenna model in front of a DTT reference scenario for a clearance of 30 mm between the separatrix and the limiter front. A dielectric constant of 225 and a loss tangent of 1.17 at 90 MHz provided the best fit. Such values partially depend on chosen antenna and its peak $n_\parallel$, and pertain to a plasma with minor differences from the latest one. Therefore, rather than allowing for an estimate of coupled power, these electromagnetic properties are intended to approximately predict the behaviour of G_{eff} versus frequency and its order of magnitude to perform a meaningful comparison between various antenna options.

ANALYSIS OF ANTENNA OPTIONS

Self-resonant antenna

This antenna concept relies on matching the electric and magnetic energies stored in the antenna box. Due to the small electrical size of the latter this resonant effect is narrow-band, but the position of the resonance can be adjusted by radially moving a mechanical tuning element. The spatial energy storage affects both matching and maximum electric fields in the antenna box in combination with other design parameters such as box volume, type of strap termination, geometrical shapes of current-carrying conductors, tap point between strap and feed, etc.

More than 30 different implementations of this concept were studied due to the ample number of degrees of freedom. Some details of this work can be found in Ref. 37, while the full analysis of an optimized launcher is presented in Ref. 38. Fig. 5 shows the results for one of the most promising implementations. Its advantages also include being a radially fixed antenna located in the port recess, i.e. very far from the plasma, fully exploiting the available room in the duct. The maximum electric field is around 3 MV/m in the worst case (tuning element close to the strap), so further work is required to make this solution suitable for DTT. While generating reflections below -10 dB in most of the intended band, its operation is expected in conjunction with some external matching network to protect the RF generators at all frequencies and for possible plasma sudden variations.
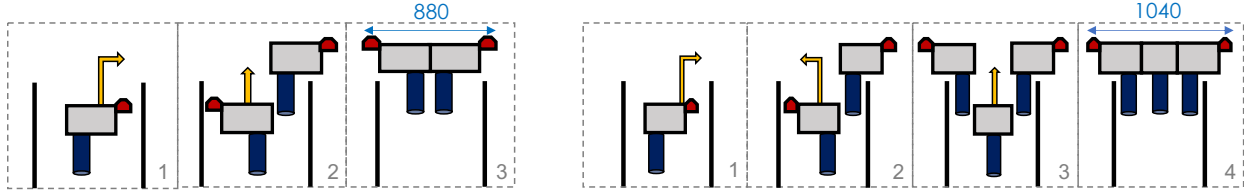
FIGURE 6. Assembling procedure of 4-strap (left) and 3-strap (right) antennas with their maximum toroidal extension in mm.
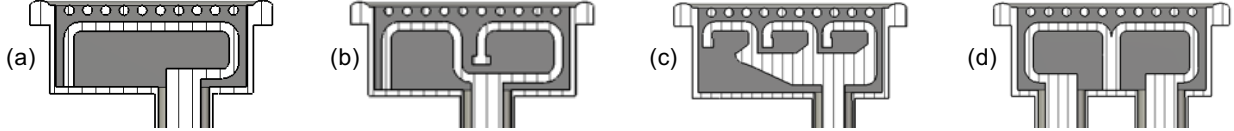

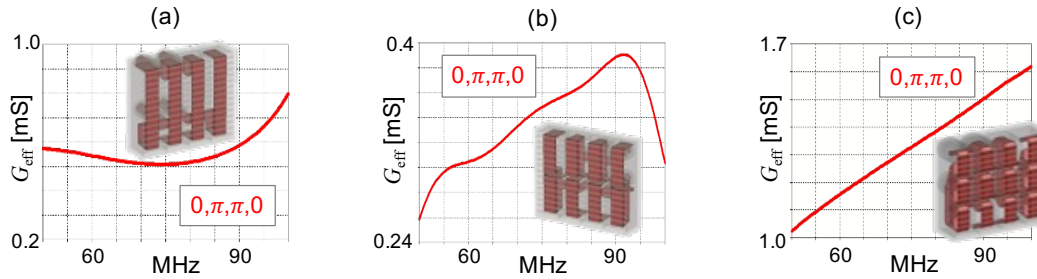**FIGURE 7.** Strap shape: straight (a), folded (b), triplet (c), end-fed centre-grounded (d).

FIGURE 8. Effective minimum conductance versus frequency of optimized 4-strap antennas deployable through ICRF ducts in the case of straight (a), folded (b), and triplet (c) straps.

4-strap and 3-strap antennas

Four- and three-strap antenna concepts were firstly studied in a form deployable through ICRF ports. The latter entails some constraints on the toroidal extension of antenna pieces, as can be grasped from Fig. 6 where some steps of the assembling procedure are depicted. The width of 4-strap antennas is limited to 880 mm; a wider geometry is feasible with 3-strap antennas, but the housing of their central strap cannot exceed 240 mm in toroidal direction. Such constraints do not apply if the remote-handling system (RHS) is charged with the assembling and disassembling of ICRF antennas. Since antennas cannot occupy adjacent sectors, a limit to their toroidal dimension remains and it is around 1080 mm. Moreover, compared to the case without RHS, the antenna poloidal dimension has to be reduced by 100 mm: the available room for the passage of antennas through RHS ducts is indeed smaller than through ICRF ducts due to the presence of additional cooling pipes of the first wall.

Three versions of 4-strap antennas were considered. They differ in the strap shape that consists of either one, two or three segments and will be referred to as straight, folded, and triplet, respectively. For 3-strap antennas, two implementations with folded lateral straps and a different central strap were considered: the one uses an end-fed, centre-grounded strap, the other a triplet. Strap shapes are sketched in Fig. 7. An in-depth description of these antenna options and their optimization can be found in Refs. 39 and 40.

The performance of optimized 4-strap geometries belonging to the group of options deployable through ICRF ports is plotted in Fig. 8. The effective minimum conductance is severely impaired by the limited toroidal extension of antennas. The same options in the version relying on RHS present a better behaviour except for the geometry with triplet straps that suffers from the reduction of antenna height to a larger extent. In general G_{eff} are always too low. For the sake of brevity, their plots are not shown, anyhow their values at 60 and 90 MHz are respectively equal to 1.47 and 1.63 mS for straight straps, 0.82 and 1.06 mS for folded straps, and 0.41 and 0.73 mS for triplet straps.

As far as 3-strap antenna geometries are concerned, their optimized G_{eff} for the installation case without RHS is
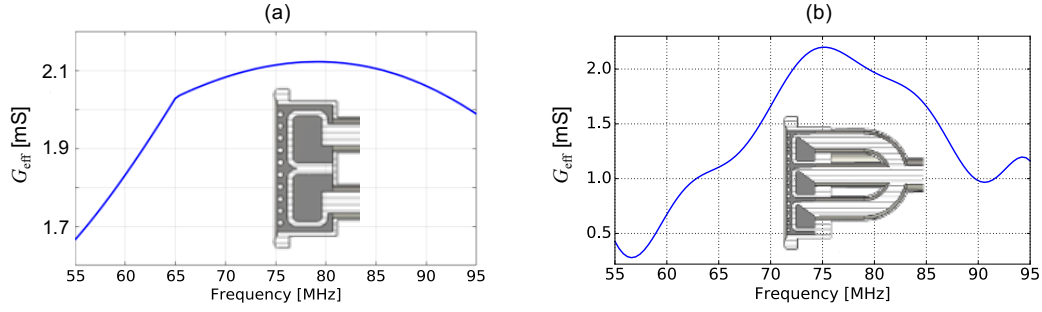
FIGURE 9. Effective minimum conductance versus frequency of optimized 3-strap antennas deployable through ICRF ducts in the case of end-fed centre-grounded (a), and triplet (b) central strap.
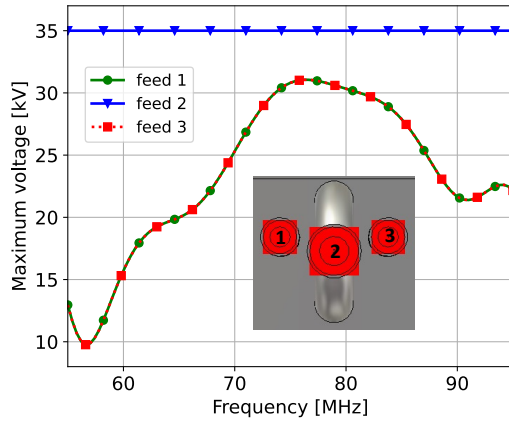

FIGURE 10. Maximum voltages in RF lines feeding the 3-strap antenna with central triplet.
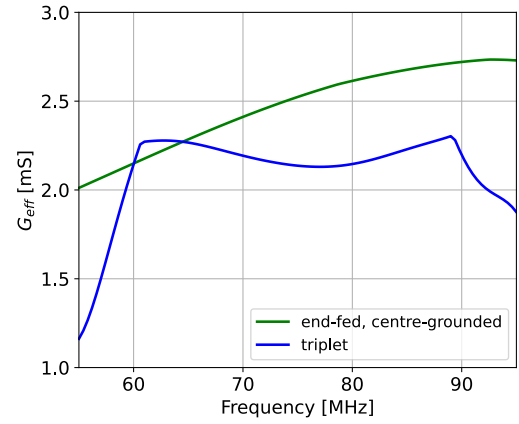

FIGURE 11. Effective minimum conductance vs. frequency of optimized 3-strap antennas relying on RHS.

shown in Fig. 9. The coupling performance, which is better than 4-strap antenna options, is limited by the constraint on the central strap width dictated by the assembling procedure. Fig. 10 depicts the maximum voltage in the feeding lines of the antenna with the central strap split in three segments. RF feeds 1 and 3 are connected to the lateral straps, while RF feed 2 to the central strap. The latter experiences high reflection due to its narrow housing, causing lateral feeding lines to work far from the standoff voltage of 35 kV. A free partition of the antenna box would allow for higher G_{eff}. Accordingly, antenna options optimized under the constraints of the RHS case achieve better performance as can be appreciated in Fig. 11. In particular the 3-strap antenna with end-fed centre-grounded central strap outperforms the other option, standing out as the preferable design for DTT between analysed traditional antenna concepts.

DETAILED RF ASSESSMENT OF THE BASELINE TRADITIONAL DESIGN

The 3-strap antenna with end-fed centre-grounded central strap was also simulated with TOPICA (TOrino Polytechnic Ion Cyclotron Antenna) code [41] to have a clear idea of its performance in DTT. The kinetic profiles of the single null, 6 T, 5.5 MA, reference scenario with neon seeding, predicted by integrated modeling simulations [17], were joint with those predicted by edge simulations in plasma detachment condition [42] and given as input to TOPICA. The outer SOL profile from the lower hybrid density to the antenna was replaced with vacuum. The equilibrium magnetic field features a tilt of around 18 deg with respect to the equatorial plane. Due to the flexibility of the magnetic configurations in DTT, a field alignment of antennas is unlikely; anyhow it would be feasible with present antenna design and could be better assessed during next design phases.

The predictions of power capability with the antenna limiter front at 20 and 40 mm from the separatrix are shown in Fig. 12. The particle energy flux flowing out of confined plasma on the outer mid plane reduces to a 5% ($\approx$
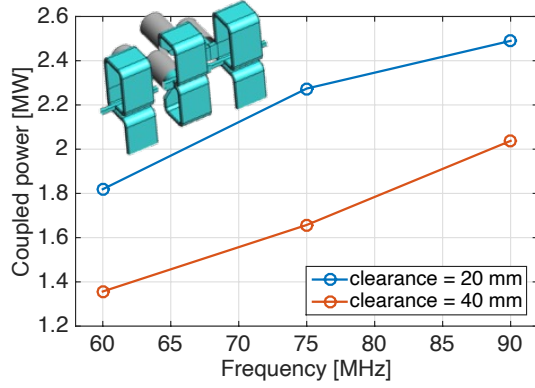
FIGURE 12. Power coupling capability of the baseline antenna design for the condition $P_C = P_L$.
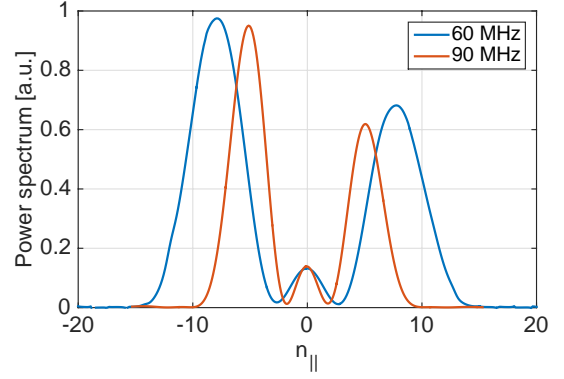

FIGURE 13. Normalized antenna power spectra at 60 and 90 MHz for a clearance of 40 mm when $P_C = P_L$.
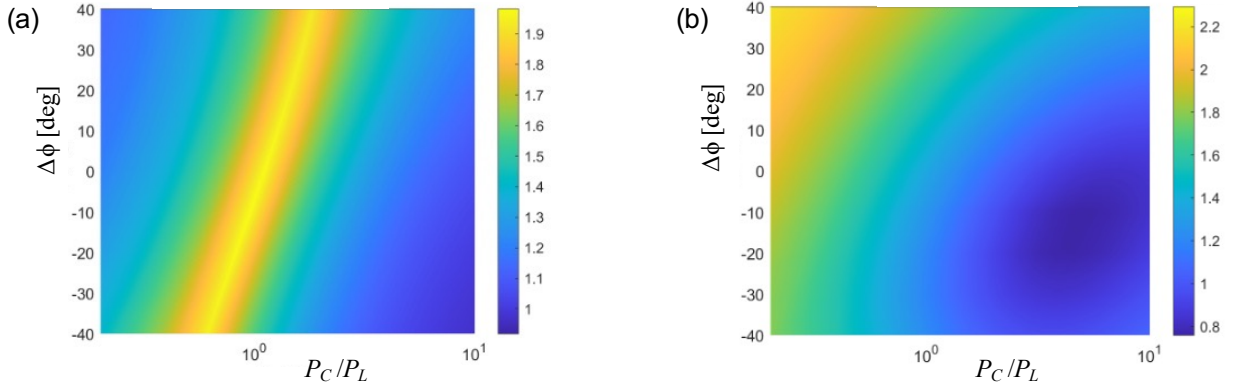

FIGURE 14. Scan of power coupling capability [MW] (a) and average $E_\parallel$ [V/m] on a rectangular area placed 3 mm in front of a side limiter for a coupled power of 1.5 MW (b) versus P_C/P_L and $\Delta\phi$ at 60 MHz with a clearance of 20 mm.

$3\lambda_q$) at a distance of 10 mm from the separatrix, therefore a clearance of 20 mm is already a safe value for ICRF antennas. However, this baseline design presents a large margin with reference to the requirement of 1.5 MW per antenna, allowing for operations further than 20 mm from the separatrix at most frequencies. Further improvements to the coupling performance are feasible, e.g., by considering a re-allocation of cooling pipes in vessel ducts, which currently constrain the height of antenna options based on the RHS. Nevertheless the strategy is to exploit all room for improvement to reduce unwanted RF interactions in the plasma edge by optimizing the present design in terms of power spectrum and $\langle E_\parallel \rangle$. As to the former, Fig. 13 depicts the cuts for $n_{\text{poloidal}} = 0$ at the boundaries of the frequency range, showing the need to minimize the power coupled in the $|n_\parallel| < 1$ domain [43]. At to the latter, Fig. 14 shows the coupled power and $\langle E_\parallel \rangle$ as a function of the power balance between central and lateral straps (P_C/P_L), and of the antenna phasing ($\Delta\phi \, \pi \, \Delta\phi$). The values of $\langle E_\parallel \rangle$ are rather low, but an optimal design is expected to have the minimum closer to the operational condition $P_C/P_L = 1$ and $\Delta\phi = 0$.

CONCLUSION

The basis of design for the ICRF system of DTT has been described and several antenna options have been assessed to identify the most suitable one. A tunable self-resonant antenna is undoubtedly the most promising concept, but it requires further investigation and R&D work, so it can be only pursued on a longer timescale for a second couple of DTT antennas. Among considered traditional solutions, the best candidate is instead the 3-strap concept with four

feeds, folded lateral straps and an end-fed center-grounded central strap. A deeper analysis of this option has been carried out with TOPICA to check its compliance with DTT requirements and declare it as the baseline design.

ACKNOWLEDGMENTS

REFERENCES

1. J.-M. Noterdaeme, AIP Conf. Proc. **2254**, 020001 (2020).
2. W. Zhang *et al.*, Nucl. Fusion **62**, 076045 (2022).
3. V. Bobkov *et al.*, Nucl. Fusion **61**, 046039 (2021).
4. F. Durodié *et al.*, AIP Conf. Proc. **1580**, 362–365 (2014).
5. Y. Lin, J. C. Wright, and S. J. Wukitch, J. Plasma Phys. **86**, 865860506 (2020).
6. F. Louche *et al.*, Fusion Eng. Des. **96-97**, 508–511 (2015).
7. R. Ambrosino, Fusion Eng. Des. **167**, 112330 (2021).
8. W. Helou *et al.*, Fusion Eng. Des. **96-97**, 473–476 (2015).
9. S. J. Wukitch *et al.*, AIP Conf. Proc. **1580**, 73–80 (2014).
10. V. Bobkov *et al.*, Plasma Phys. Control. Fusion **59**, 014022 (2016).
11. R. Ragona *et al.*, Nucl. Fusion **60**, 016027 (2019).
12. S. Ceccuzzi *et al.*, Fusion Eng. Des. **146**, 361–364 (2019).
13. V. Bobkov *et al.*, Nucl. Mater. Energy **18**, 131–140 (2019).
14. A. Lyssoivan *et al.*, Plasma Phys. Control. Fusion **54**, 074014 (2012).
15. Y. O. Kazakov *et al.*, Nat. Phys. **13**, 973–978 (2017).
16. A. Cardinali *et al.*, "Numerical investigation of the ion cyclotron resonance heating (ICRH) physics in DTT," (2022), proc. of the Joint Varenna–Lausanne International Workshop on Theory of Fusion Plasmas, September 12-16, 2022, Varenna, Italy (unpublished).
17. I. Casiraghi *et al.*, Nucl. Fusion **61**, 116068 (2021).
18. A. Cardinali *et al.*, Plasma Phys. Control. Fusion **62**, 044001 (2020).
19. G. L. Ravera *et al.*, "Operational requirements of the ion cyclotron wall conditioning in DTT," (2022), proc. of the 32nd Symposium of Fusion Technology, September 18-23, 2022, Dubrovnik, Croatia (unpublished).
20. F. Durodié *et al.*, "Latest achievements of the JET ICRF systems in view of ITER," in *Proc. of the 23rd IAEA FEC* (2010).
21. M. Graham *et al.*, Plasma Phys. Control. Fusion **54**, 074011 (2012).
22. H. Faugel, V. Bobkov, and H. Fünfgelder, AIP Conf. Proc. **2254**, 070006 (2020).
23. Y. Zhao *et al.*, Fusion Eng. Des. **89**, 2642–2646 (2014).
24. G. Haste *et al.*, Fusion Eng. Des. **24**, 191–204 (1994).
25. S. J. Wukitch *et al.*, Plasma Phys. Control. Fusion **46**, 1479–1491 (2004).
26. A. Kaye *et al.*, Fusion Eng. Des. **24**, 1–21 (1994).
27. F. Durodié *et al.*, Plasma Phys. Control. Fusion **54**, 074012 (2012).
28. D. J. Hoffman *et al.*, AIP Conf. Proc. **159**, 302–305 (1987).
29. V. Bobkov, J.-M. Noterdaeme, F. Wesner, R. Wilhelm, and ASDEX Upgrade Team, J. Nucl. Mater. **313-316**, 956–961 (2003).
30. H. Kimura *et al.*, Fusion Eng. Des. **26**, 95–102 (1995).
31. K. Vulliez *et al.*, Fusion Eng. Des. **74**, 267–271 (2005).
32. W. Tierens, J. Jacquot, V. Bobkov, J. Noterdaeme, and L. Colas, Nucl. Fusion **57**, 116034 (2017).
33. S. Ceccuzzi, A. Cardinali, G. L. Ravera, and A. A. Tuccillo, AIP Conf. Proc. **2254**, 050004 (2020).
34. G. Torrisi, D. Mascali, G. Sorbello, G. Castro, L. Celona, and S. Gammino, IEEE Trans. Antennas Propag. **67**, 2142–2149 (2019).
35. D. Milanesio, O. Meneghini, V. Lancellotti, R. Maggiora, and G. Vecchi, Nucl. Fusion **49**, 115019 (2009).
36. G. Torrisi *et al.*, "Development/extension of a COMSOL full-wave anisotropic model for the ICRH heating," (2022), this conference.
37. D. Milanesio *et al.*, "A self-resonant plug-in IC antenna for DTT," (2022), this conference.
38. D. Milanesio *et al.*, "Design of a tunable resonant antenna for DTT experiment," (2022), Nucl. Fusion (to be submitted).
39. G. S. Mauro *et al.*, "Numerical design and optimization of a three-strap antenna for DTT IC heating," (2022), proc. of the 32nd Symposium of Fusion Technology, September 18-23, 2022, Dubrovnik, Croatia (unpublished).
40. F. Mirizzi *et al.*, "Preliminary analyses of the ICRF launcher for DTT," (2022), proc. of the 32nd Symposium of Fusion Technology, September 18-23, 2022, Dubrovnik, Croatia (unpublished).
41. V. Lancellotti, D. Milanesio, R. Maggiora, G. Vecchi, and V. Kyrytsya, Nucl. Fusion **46**, S476–S499 (2006).
42. P. Innocente *et al.*, "Design of a multi-configurations divertor for the DTT facility," (2022), j. Nucl. Mater. (submitted).
43. A. Messiaen and V. Maquet, Nucl. Fusion **60**, 076014 (2020).